NANO EXPRESS

Silver Nanoparticles and Graphitic Carbon Through Thermal Decomposition of a Silver/Acetylenedicarboxylic Salt

**Panagiotis Dallas · Athanasios B. Bourlinos ·
Philomela Komninou · Michael Karakassides ·
Dimitrios Niarchos**

Abstract Spherically shaped silver nanoparticles embedded in a carbon matrix were synthesized by thermal decomposition of a Ag(I)/acetylenedicarboxylic acid salt. The silver nanoparticles, which are formed either by pyrolysis at 300 °C in an autoclave or thermolysis in xylene suspension at reflux temperature, are acting catalytically for the formation of graphite layers. Both reactions proceed through in situ reduction of the silver cations and polymerization of the central acetylene triple bonds and the exact temperature of the reaction can be monitored through DTA analysis. Interestingly, the thermal decomposition of this silver salt in xylene partly leads to a minor fraction of quasicrystalline silver, as established by HR-TEM analysis. The graphitic layers covering the silver nanoparticles are clearly seen in HR-TEM images and, furthermore, established by the presence of sp^2 carbon at the Raman spectrum of both samples.

Keywords Silver nanoparticles · Graphitization · Acetylenedicarboxylic acid · Nanocomposites

P. Dallas (✉) · A. B. Bourlinos (✉) · D. Niarchos
Institute of Materials Science, NCSR 'Demokritos',
15310 Athens, Greece
e-mail: dallas@demokritos.com; dallas@ims.demokritos.gr;
panosdallas@gmail.com

A. B. Bourlinos
e-mail: bourlinos@ims.demokritos.gr

P. Komninou
Department of Physics, Aristotle University of Thessaloniki,
Thessaloniki, Greece

M. Karakassides
Department of Materials Science and Engineering,
University of Ioannina, Ioannina, Greece

Introduction

Acetylenedicarboxylic acid (ACD) as carboxylic acids with short aliphatic chains [1] is well known to form complexes with transition metals such as Cd(II) [2], Cu(II) [3], Mn(II) [4] or even lanthanide cations [5] either in single crystal or in powder form. The metal cations are coordinated with both carboxylate groups in a chelating mode, thus forming metal-organic chains. Interestingly, the triple bond centered between the carboxylate units of acetylenedicarboxylic acid provides new design parameters for the synthesis of novel structures since the distance between the ligands can be decreased enough to succeed polymerization leading to conjugated materials as demonstrated by Skoulika et al. [6]. As such, acetylenedicarboxylic acid is a promising candidate for the synthesis of novel metal-organic networks with interesting properties. Nonetheless, the derived carbon materials obtained after thermal decomposition of such complexes are yet to be the target of intense research, especially considering that the acetylene unit provides an excellent source for carbon, whereas the central metal cation may act as a catalyst.

On the other hand, in another research field, the field of nanoscience, applications of noble-metal nanoparticles, especially silver, have recently grown exponentially. Silver nanoparticles display unique physical, chemical [7–9], and biologic properties such as high antibacterial activity toward a large number of bacterial strains [10, 11] and furthermore they have been incorporated in various natural [12], conductive [13] or dendritic [14] polymer matrices toward the synthesis of advanced nanocomposite materials. Besides the above mentioned colloidal nanocrystals and polymer nanocomposites, carbon-supported silver metal nanoparticles exhibit a wide range of applications in catalysis, antibacterial activity, thermal conductivity, and

electronic materials [15, 16]. These hybrid materials are usually obtained by impregnation of a presynthesized carbon support with silver salts and subsequent reduction to silver metal (i.e., a multistep process). Accordingly, the one-step fabrication of silver–carbon hybrids would be much recommended and is highly anticipated.

Recently, an interesting procedure has been proposed describing the catalytic growth of crystalline graphite through thermal decomposition of an organometallic iron complex in solution [17]. This process leads to the catalytic graphitization of the organic component and simultaneously to the formation of magnetic iron oxide nanoparticles. This synthetic route seems to be of high importance since the graphitization process usually demands high temperatures, typically in the range 500–1,000 °C [18–20]. To that direction, herein we report an entirely different but conceptually relevant case of catalytic graphitization based on the thermal decomposition of the silver acetylenedicarboxylate salt, which leads to the reduction of silver cations to metallic nanoparticles and the simultaneous formation of a carbon coating. Two different processes have been employed involving either thermolysis of the silver salt or thermal decomposition in the solid state. Given the dramatic effect of several metal nanoparticles on the growth and morphology of a series of intriguing carbon nanostructures, the direct thermal decomposition of suitable organometallic precursors may give an easy access to metal-carbon nanocomposites as well as carbogenic nanostructures with emergent morphologies.

Experimental Section (Scheme 1)

Synthesis of Silver/Acetylenedicarboxylic Salt

The experimental details involve in the first step the synthesis of the precursor salt of Ag(I) with acetylenedicarboxylic acid, (ACD), (Aldrich, 95%). About 425 mg of $AgNO_3$ (Riedel De Haan, 99.5%) was dissolved in 15 mL H_2O and an aqueous solution of 280 mg ACD (15 mL H_2O) was slowly added. A white precipitate was formed immediately. The solid was easily isolated by centrifugation,
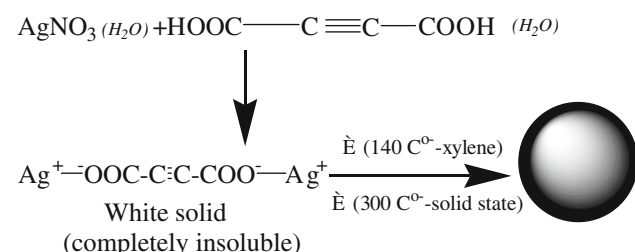
washed with water several times in order to remove residual salts and organics, and finally dried at 50 °C for 24 h away from light. Sample name: Ag/ACD.

Thermolysis of Ag/ACD in Xylene

The white Ag/ACD powder (200 mg) was suspended in xylene (30 mL) and refluxed for 1 h. Within few minutes the color of the suspended solid changed from white to black. The reaction is completed in much lower temperatures than the boiling point of xylene (140 °C) as evidenced by DTA analysis of the Ag/ACD salt (Fig. 6a). After reaction accomplishment, the black powder was isolated by centrifugation, washed with alcohol and acetone several times, and dried at 50 °C for 24 h. Sample name: Ag/sol.

Thermal Decomposition of Ag/ACD in the Solid State

Ag/ACD white powder (1 g) was loaded in Teflon equipped stainless steel autoclave and the sealed system was heated at 300 °C for 2 h at a heating rate of 10 °C min^{-1}. The black powder was washed numerous times with water and acetone prior to drying. Sample name: Ag/pyr.

Characterization Techniques

XRD patterns were recorded on powder samples using a Siemens 500 Diffractometer. Cu Kα radiation was used with a scan rate 0.03 s^{-1}. Thermogravimetric and Differential thermal analysis measurements were recorded on a Perkin–Elmer Pyris TGA/DTA under airflow with a heating rate 10 °C min^{-1}. Infrared spectra were taken on KBr (Aldrich, 99%, FT-IR grade) pellets with a FT-IR spectrometer of Bruker, Equinox 55/S 123 model. The UV–visible spectrum was recorded on a Shimadzu 2100 spectrometer using ethanol suspensions in quartz cuvettes. The Raman spectra were recorded using a Raman microscope system (Renishaw, System 1000) consisting of an optical microscope (Leica) coupled to a Raman spectrometer (532 nm).

$$AgNO_{3\ (H_2O)} + HOOC\!-\!\!-\!\!C \equiv C\!-\!\!-\!COOH \quad {}_{(H_2O)}$$

$$Ag^+\!-\!OOC\text{-}C\vdots C\text{-}COO^-\!-\!Ag^+ \quad \xrightarrow[\grave{E}\ (300\ C^{o}\text{-solid state})]{\grave{E}\ (140\ C^{o}\text{-xylene})}$$

White solid
(completely insoluble)

Scheme 1 A schematic representation of the reaction steps

Results and Discussion

Synthesis, FT-IR and Raman Spectroscopy

Each carboxylate anion unit of the acetylenedicarboxylic acid coordinates easily with a silver cation, leading to a fast precipitation process almost immediately after the addition of the reagents. The white powder that is formed signals the formation of the precursor silver salt that was first

Fig. 1 FT-IR spectra of **a** Ag/sol, **b** ACD, **c** Ag/ACD, **d** Ag/pyr
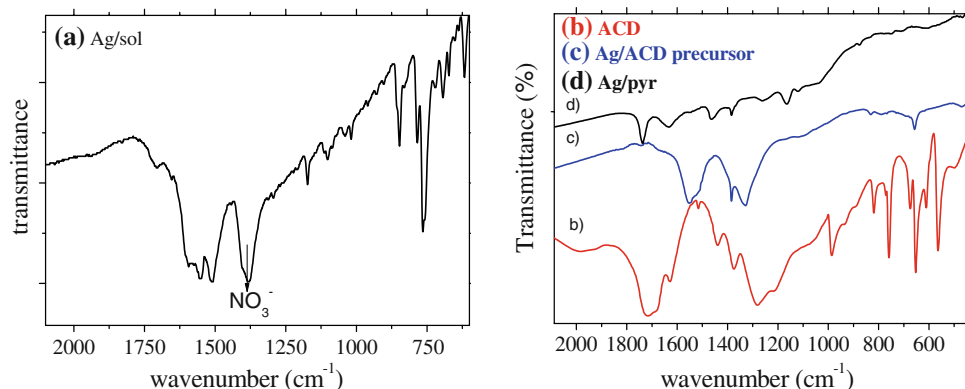

characterized using FT-IR spectroscopy (Fig. 1). The spectra of the ACD and Ag/ACD are significantly different, clearly indicating the coordination of both carboxylate anions with silver cations. The vibration mode centered at 1,700 cm^{-1} is assigned to a dimer between two saturated carboxylic groups of the ACD, while at the Ag/ACD complex spectrum, the antisymmetric and symmetric vibration modes of the carboxylate anion appear and are located at 1,551 and 1,342 cm^{-1}, respectively. The difference between the frequencies of these two bands is 209 cm^{-1}, which indicates "pseudo-unidentate" coordination between the metal sites and the carboxylate anions [21]. Furthermore, the absence of a peak assigned to –COOH units in the spectrum of the precursor salt, Ag/ACD, indicates that all acetylenedicarboxylic moieties are in anionic form coordinated with silver cations. If the sample is dried and left as it is, after a few days it obtains a yellow color, which can be assigned to an interaction of Ag$^+$ with acetylene units [22]. After thermal decomposition of Ag/ACD in the solid state, the IR spectrum of the corresponding Ag/pyr is exhibiting a spectrum with a weak absorption band at 1,732 cm^{-1} attributed to C=O groups as well as weak and broad absorption in the range 1,600–1,000 cm^{-1} ascribed to oxygen-containing functional groups (e.g., C–OH, C–O–C and residual carboxylates) and carbon double bonds (e.g., from partially unsaturated rings within graphene layers). Similarly, the FT-IR spectrum of

the Ag/sol sample is quite typical for an extended carbon double bond network, with strong absorption peaks in the 1,540–1,580 cm^{-1} region. Also the presence of a strong absorption at 1,389 wavenumbers, which is well known to come from nitrate anions (NO$_3^-$), is noticed. In that case the nitrate anions should be absorbed on the surface of the nanoparticles.

Further structural information based on the acetylene triple bond was not possible to be collected due to the absence of characteristic IR signals, something that is expected in a symmetric molecule like ACD. Lastly, in a blank experiment, when neat ACD was refluxed in xylene a light yellow-brown colored solution was obtained, meaning that the graphitization is not possible in the absence of silver.

In order to establish the formation of graphitic carbon we performed Raman measurements, which are particularly useful in the identification of graphite. The diagrams corresponding to the Ag/sol and Ag/pyr samples are presented in Fig. 2. Both spectra are typical of the formation of sp^2 carbon bonds according to the appearance of a band at 1,590 cm^{-1} (G-band), while a lower percentage of sp^3 carbon bonds is indicated by the second band centered at 1,369 cm^{-1} (D-band) [23–25]. We assign the formation of the graphitic layers to a coupling reaction of the acetylene units that is catalytically promoted by the simultaneous formation of silver nanoparticles. Similarly to the role of

Fig. 2 Raman spectra of samples **a** Ag/pyr, **b** Ag/sol
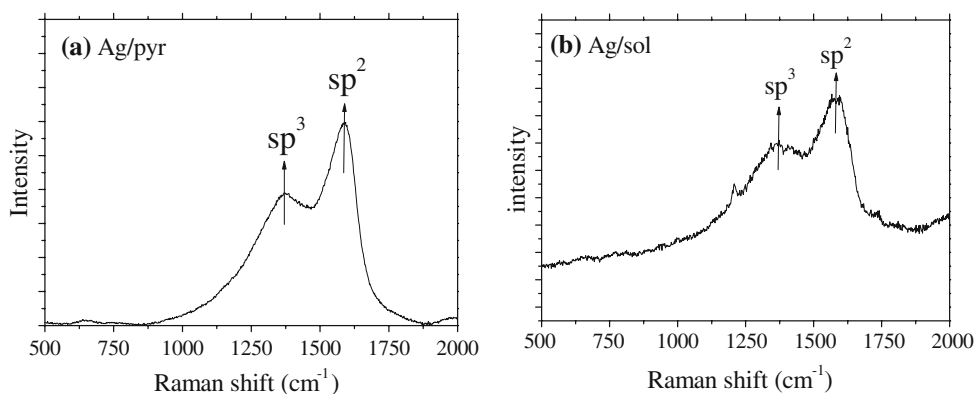
iron oxide nanoparticles in the procedure published by Walter et al. [17], we propose that the silver nanoparticles facilitate the reaction among the acetylene units at low temperatures and relatively mild conditions. For instance, the catalytic impact of silver toward graphitization has been previously demonstrated [26].

Structural and Morphological Study: XRD Analysis and Electron Microscopy

The materials were firstly characterized with XRD analysis. The XRD pattern of the precursor Ag/ACD (Fig. 3a) is characteristic of an amorphous material. The presence of two broad bands without any pronounced peak, centered in $2\theta = 11°$ and $2\theta = 32°$ may be assigned to the glass support holder and the silver salt, respectively. Since the band is significantly broad, the material cannot be considered to exhibit any symmetric ordering and should be characterized as amorphous. After thermal decomposition of the precursor in the solid state, the XRD study establishes the formation of highly crystalline silver nanoparticles in Ag/pyr (Fig. 3b). The small carbon fraction in Ag/pyr (based on TGA measurements) and the density contrast between carbon and silver (i.e., carbon filaments

are much lighter) made difficult the observation of the carbon phase in this sample. Additionally, the XRD pattern of Ag/sol obtained by thermolysis of Ag/ACD in xylene also establishes the complete formation of metallic silver nanoparticles (Fig. 3c). The pattern of the Ag/sol sample exhibits one extra peak compared to the Ag/pyr pattern, which is centered at $2\theta = 28.8$ Å. This value is consistent with the arrangement of turbostratic carbon filaments [27] and it is quite close to the characteristic interplanar spacing of graphite (d spacing at 3.35 Å) [28]. Likewise Ag/pyr, the small carbon fraction and large scattering factor of silver are responsible for the weak intensity of graphite peak in Ag/sol. A mean particle size D can be deduced by applying the Scherrer equation at the strongest peak of the XRD pattern [29, 30], $D = 0.9\lambda/\Delta(2\theta)\cos\theta$, where D is the crystalline domain size, $\Delta(2\theta)$ is the full width at half maximum of the strongest peak and λ is the X Ray wavelength ($\lambda = 1.5418$ Å), and it is roughly estimated to be about 30 nm and 20 nm for the Ag/pyr and Ag/sol sample, respectively, revealing a moderate size distribution for both samples.

After establishing the complete decomposition of the silver salt and reduction of the cations toward silver nanoparticles, we employed TEM microscopy in order to

Fig. 3 XRD patterns of all samples: **a** Ag/ACD, **b** Ag/pyr and **c** Ag/sol. The hkl indices of the metallic silver are indicated
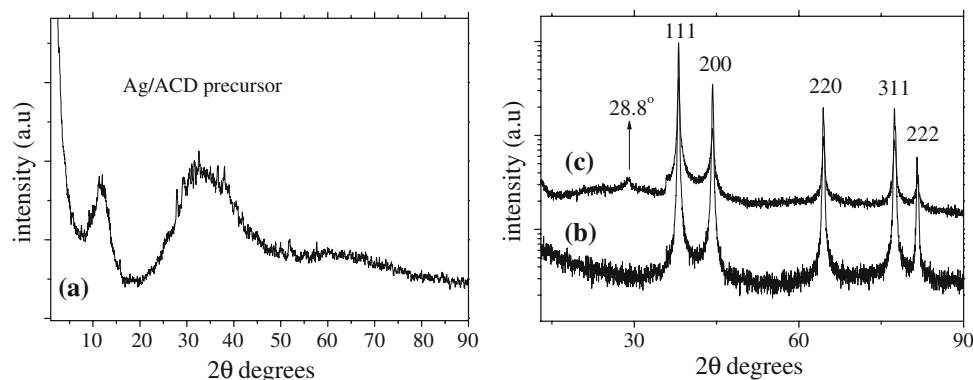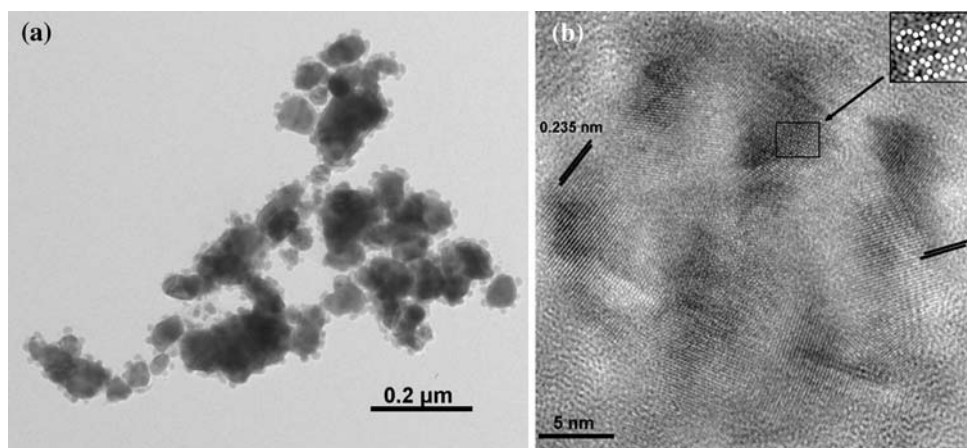

Fig. 4 **a** HR-TEM image of the Ag/sol sample. **b** The corresponding HR-TEM analysis of an individual nanoparticle. The quasicrystalline phase is marked and shown as *inset*. It is a minor percentage of the overall crystal. The carbon coating can be seen surrounding the silver crystal

fully characterize the samples. Besides the expected presence of spherical silver nanoparticles, two interesting aspects should be marked in the TEM analysis of both samples: the appearance of turbostratic graphitic layers at the Ag/pyr sample and a minor fraction of quasicrystalline cubic silver phase in the Ag/sol (Figs. 4, 5). Quasicrystals emerged in the field of materials science in 1984 when an unexpected fivefold symmetry in the electron diffraction pattern of an Al–Mn alloy was observed [31]. Later on, many alloys with a quasicrystalline phase have been synthesized and extensively characterized, and even natural occurring quasicrystals have been recently found and studied [32], but to our knowledge this is the first report for a fivefold symmetry in noble metal nanocrystals. However, the mechanism that leads to this completely unexpected symmetry is yet to be revealed and in any case the quasicrystalline phase is a minor percent of the overall material.

Secondly, in the Ag/pyr sample, curved graphitic filaments are revealed in the HR-TEM images (Fig. 5) forming a matrix where the silver nanoparticles are hosted. The curvature of the carbon filaments is more pronounced near the edges and can be ascribed to the previously reported catalytic effect of silver nanoparticles on the growth of carbon onions [26]. The silver nanoparticles seem to be the core areas of the composite, which are interconnected by the carbon layers. This is in accordance with the reaction steps that we propose, where the formation of silver

nanoparticles is the catalytic step for the polymerization of the central acetylene units. And in fact, the pyrolytic process is much closer to this mechanism than the solvothermal, most probably due to the low reaction time and violent conditions that are taking place inside the autoclave.

Thermal Analysis

Firstly, the exact reaction point and thermal decomposition of the silver/acetylenedicarboxylic salt was evaluated through DTA analysis. The curve (Fig. 6a) shows a strong exothermic process starting from 110 °C and reaching its maximum peak at 132 °C, with an enthalpy flow approximately -103 μV s/mg. Compared to the simple acetylenedicarboxylic acid, which has a melting point (decomposition) at 180 °C, the silver salt is significantly more active. Unfortunately the thermal decomposition of this salt is extremely violent and explosive and the TGA curves could not be recorded since this thermogravimetric measurement exhibits extreme noise and it can even damage the TG balance.

The weight percentages of carbon and silver in both samples were obtained with thermogravimetric analysis under airflow. The TGA/DTA diagrams for the two composites are presented in Fig. 6. The traces of the Ag/pyr sample present a weight loss due to the thermal decomposition of the carbon layer, starting at 300 °C and

Fig. 5 HR-TEM images of the Ag/pyr sample. The graphitic layers can be seen surrounding the individual silver nanoparticles, thus forming a carbon matrix where the nanoparticles are encapsulated. In the *last image* a single silver nanoparticle and its typical interlayer spacing is shown in magnification
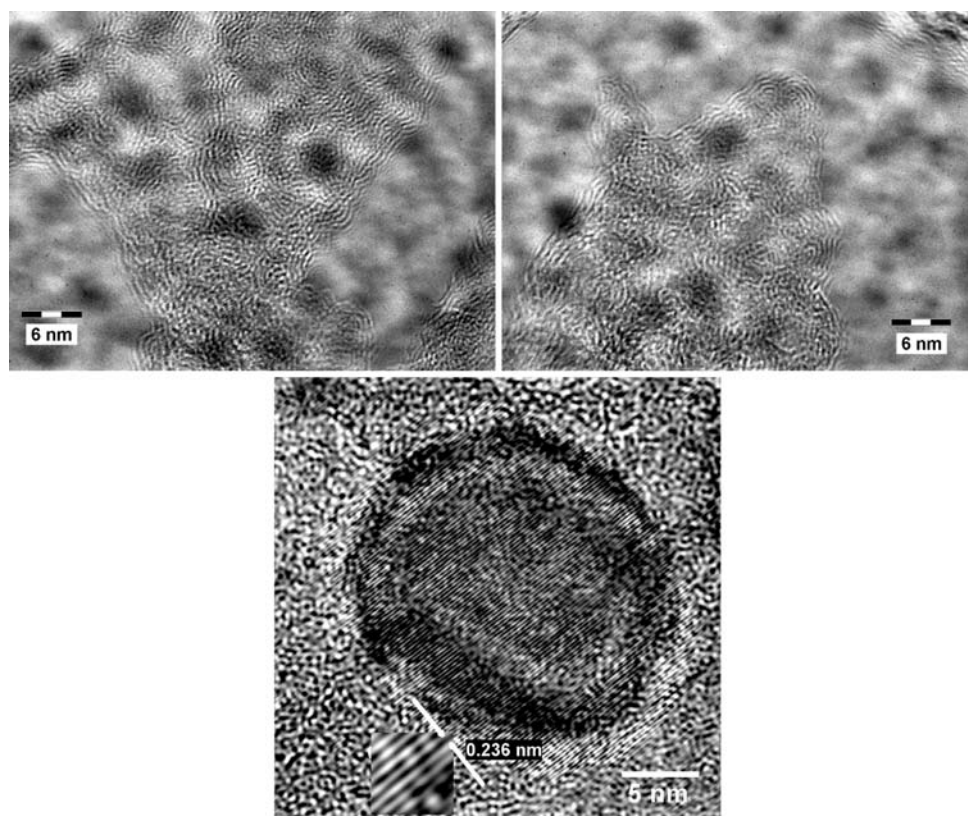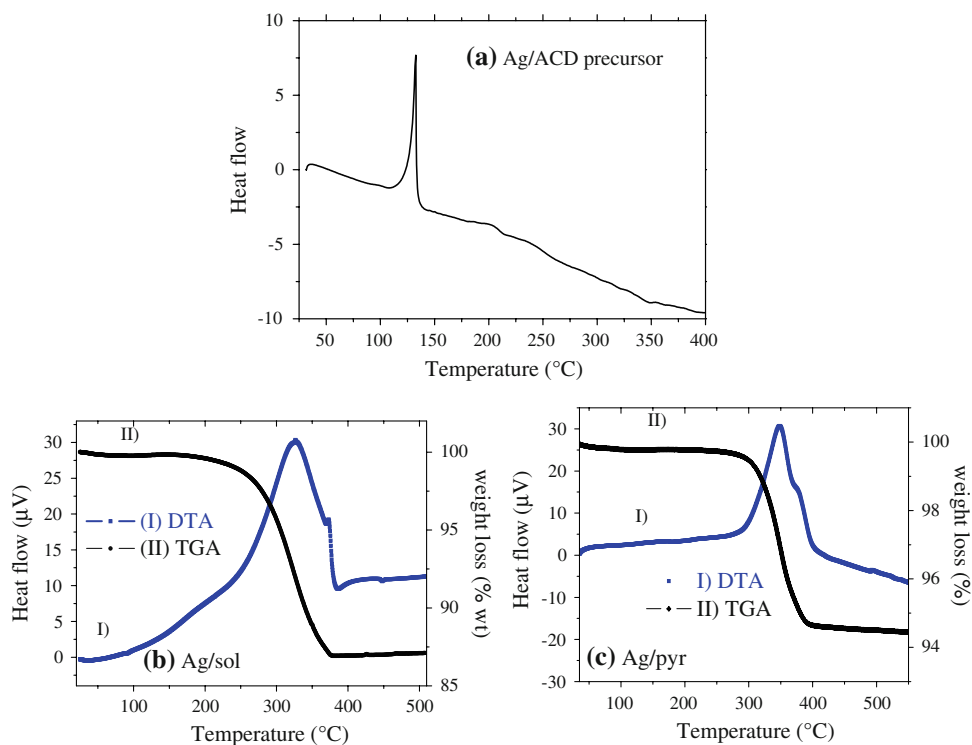
completed at 400 °C. A sharp exothermic peak in the DTA diagram, which is centered at 349 °C, also marks this thermal decomposition. Accordingly, the calculated weight percentage of the silver nanoparticles is about 94% wt and remains a 6% wt which can be assigned to the carbon coating. A similar thermogravimetric analysis curve is obtained for the Ag/sol sample with the weight percentage of carbon being significantly higher ($\sim$13% wt) most probably due to the lower reaction temperature in refluxing xylene. The corresponding DTA exothermic peak is quite the same with that of the Ag/pyr sample and it is centered at 332 °C. It should be noted that during the thermogravimetric analysis measurements and the exposure of the samples to oxygen, most probably a minor percentage of silver is oxidized to silver oxide (Ag_2O) near the surface of the nanoparticles. Therefore, it is difficult to establish precisely the silver content of the composites by TGA. However, since silver is significantly heavier than oxygen and the oxidation takes place exclusively near the surface of the nanoparticles, any formation of silver oxide should be considered negligible and without seriously affecting our calculations regarding the silver content.

UV–Visible Spectroscopy

The UV–Visible spectrum of the Ag/sol sample was recorded and is presented in Fig. 7. The spectrum was recorded in fine dispersion in ethanol after high dilution and sonication. As it is well known, silver nanoparticles

exhibit an absorption in the UV–Visible region due to their characteristic surface plasmon resonance frequency. The spectrum consists of two broad bands centered at 385 (=3.22 eV) and 770 nm (=1.61 eV). The strong absorption peak centered at 385 nm is well typical for spherically shaped silver nanoparticles [33]. However, it is slightly shifted toward lower wavelengths due to the coupling of the surface plasmon electrons with the sp^2 carbon atoms of the graphitic layers, in analogy with oligothiophene-coated gold nanoparticles [34]. Interestingly, the second, very weak, band is centered at exactly the half frequency compared to the first band (770 and 385 nm, respectively)
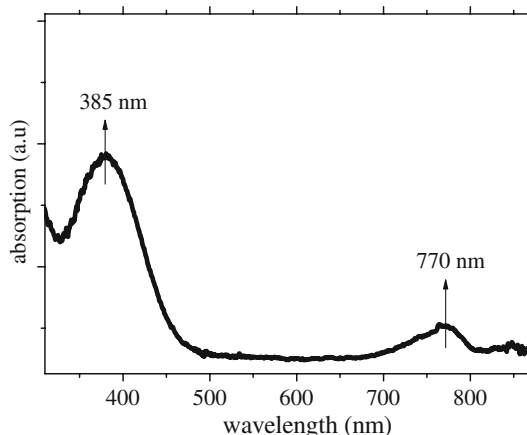

Fig. 7 UV–Visible absorption spectrum of a fine suspension of Ag/sol in ethanol

and it can be assigned to the in-plane dipole resonance of the silver nanoparticles [7]. Unlike Ag/sol, the Ag/pyr sample was completely insoluble in any solvent and hence the absorption spectrum could not be recorded.

Conclusions

An insoluble, white, Ag(I) salt with acetylenedicarboxylic acid was synthesized and used for the preparation of two silver–carbon nanocomposites via different synthetic routes. As it is indicated from the XRD patterns and TEM images both reactions lead to the formation of silver nanoparticles embedded in a carbon matrix. The graphitization proved to be much better in the solid-state reaction than in solution, however, the carbon yield is relatively lower, the reaction temperature is higher and the interesting fivefold symmetry in the silver nanoparticles is absent. As a future step toward expansion of this procedure, the violent reaction between a functional molecule like ACD and coordinated metal ions can lead to various interesting morphologies as well as nanostructures.

References

1. E.G. Bakalbassis, M. Korabik, A. Michaelides, J. Mrozinski, C. Raptopoulou, S. Skoulika, A. Terzis, D. Tsaousis, J. Chem. Soc. Dalton Trans. 850 (2001)
2. A. Michaelides, D. Tsaousis, S. Skoulika, C. Raptopoulou, A. Terzis, Acta Crystallogr. Sect. B. Struct. Sci. **54**, 657 (1998)
3. M.X. Li, M. Shao, H. Dai, B.L. An, W.C. Lu, Y. Zhu, C.X. Du, Chin. Chem. Lett. **16**(10), 1405 (2005)
4. M. Shao, M.X. Li, H. Dai, W.C. Lu, B.L. An, J. Mol. Struct. **829**, 155 (2007)
5. G. Zhang, Q. Wang, Y. Qian, G. Yang, J.S. Ma, J. Mol. Struct. **796**, 187 (2006)
6. St. Skoulika, P. Dallas, M.G. Siskos, Y. Deligiannakis, A. Michaelides, Chem. Mater. **15**, 24–4576 (2003)
7. R. Jin, Y.C. Cao, E. Hao, G.S. Metraux, G.C. Schatz, C.A. Mirkin, Nature. **425**, 487 (2003)
8. Q. Zeng, X. Jiang, A. Yu, G. Lu, Nanotechnology. **18**, 35708 (2007)
9. S. Navaladian, B. Viswanathan, R.P. Viswanath, T.K. Varadarajan, Nanoscale Res. Lett. **2**, 44 (2007)
10. A. Panacek, L. Kvitek, R. Prucek, M. Kolar, R. Vecerova, N. Pizurova, V.K. Sharma, T. Nevezna, R. Zboril, J. Phys. Chem. B. **110**, 16248 (2006)
11. L. Kvitek, A. Panacek, J. Soukopova, M. Kolar, R. Vecerova, R. Prucek, M. Holecova, R. Zboril, J. Phys. Chem. C. **112**, 5825 (2008)
12. R.J.B. Pinto, P.A.A.P. Marques, C.P. Neto, T. Trindade, S. Daina, P. Sadocco, Acta Biomater. **5**, 2279 (2009)
13. P. Dallas, D. Niarchos, D. Vrbanic, N. Boukos, S. Pejovnik, C. Trapalis, D. Petridis, Polymer. **48**, 2007 (2007)
14. M. Gladitz, S. Reinemann, H.J. Radusch, Macromol. Mater. Eng. **294**, 178 (2009)
15. C.-K. Leong, D.D.L. Chung, Carbon. **42**, 2323 (2004)
16. E. Borowiak-Palen, M.H. Ruemmeli, T. Gemming, T. Pichler, R. Jkalenczuk, S.R.P. Silva, Nanotechnology. **17**, 2415 (2006)
17. E.C. Walter, T. Beetz, M.Y. Sfeir, L.E. Brus, M.L. Steigerwald, J. Am. Chem. Soc. **128**, 15590 (2006)
18. J. Hu, Y. Bando, J. Zhan, C. Zhi, F. Xu, D. Goldberg, Adv. Mater. **18**, 197 (2006)
19. A. Govindaraj, C.N.R. Rao, Pure Appl. Chem. **74**, 1571 (2002)
20. L. Zhi, J. Wu, J. Li, U. Kolb, K. Mullen, Angew. Chem. Int. Ed. **44**, 2120 (2005)
21. G.B. Deacon, R.J. Philips, Coord. Chem. Rev. **33**, 227 (1980)
22. F. Albert Cotton, G. Wilkinson, *Advance Inorganic Chemistry* (Interscience, London, 1962)
23. A.C. Ferrari, J. Robertson, Phys. Rev. B. **61**, 14095 (2000)
24. F. Tuinstra, J.L. Koenig, J. Chem. Phys. **53**, 1126 (1970)
25. M.S. Dresselhaus, G. Dresselhaus, A. Jorio, A.G. Souza Filho, M.A. Pimenta, R. Satio, Acc. Chem. Res. **35**, 1070 (2002)
26. Th. Cabioc'h, E. Thune, M. Jaouen, Phys. Rev. B. **65**, 132103 (2002)
27. H. Song, X. Chen, X. Chen, S. Zhang, H. Li, Carbon. **41**, 3037 (2003)
28. A.H.R. Palser, Phys. Chem. Chem. Phys. **1**, 4459 (1999)
29. H.P. Klug, L.E. Alexander, *X Ray Diffraction Procedures for Polycrystalline and Amorphous Materials* (Wiley, New York, 1962), pp. 491–538
30. P. Dallas, V. Georgakilas, D. Niarchos, Ph. Komninou, Th. Kehagias, D. Petridis, Nanotechnology. **17**, 2046 (2006)
31. A.P. Tsai, Acc. Chem. Res. **36**, 31 (2003)
32. L. Bindi, P.J. Steinhart, N. Yao, P.J. Lu, Nature. **324**, 1306 (2009)
33. K.L. Kelly, E. Coronado, L.L. Zhao, G.C. Schatz, J. Phys. Chem. B. **107**, 668 (2003)
34. B.C. Sih, M.O. Wolf, J. Phys. Chem. B. **110**, 22298 (2006)